Structure and Thermal Stability of Langmuir–Blodgett–Kuhn Layers of Hairy-Rod Polymers Probed with Neutron and X-ray Reflectometry

Timothy R. Vierheller and Mark D. Foster*

Institute of Polymer Science, The University of Akron, Akron, Ohio 44325–3909

Albert Schmidt,† Klemens Mathauer,‡ Wolfgang Knoll,§ and Gerhard Wegner

Max-Planck-Institut für Polymerforschung, D-55021 Mainz 1, Germany

Sushil Satija and Charles F. Majkrzak

National Institute of Standards and Technology, Gaithersburg, Maryland 20899

Received May 5, 1994; Revised Manuscript Received August 15, 1994®

ABSTRACT: The microstructure and thermal stability of multilayer thin films of rodlike polyglutamate copolymers having flexible aliphatic side chains have been studied with X-ray and neutron reflectometry. The complementary sensitivity of X-rays and neutrons and the use of four different sequences of protonated and deuterated molecules provides an enhanced level of structural discrimination. Within bilayers formed upon deposition, the backbones are located preferentially near the center, with backbones from the two layers overlapping strongly. The side chains of molecules in adjacent layers belonging to different bilayers interdigitate substantially, and interdigitation between layers within a bilayer is seen as well. Upon annealing at 70 or 84 °C, the backbone positions within each bilayer relax. However, there is no ascertainable interlayer interdiffusion and the nature of the side chain interdigitation does not change. No evidence is found for the formation, with annealing, of a three-dimensional ordered structure.

Introduction

Rodlike polypeptide copolymers with covalently attached flexible side chains have recently been studied for use in nanostructured systems created using Langmuir–Blodgett–Kuhn (LBK) deposition.[1,2] These materials show promise for use in photonics, optoelectronics, and chemical sensors because of their unique physical properties.[1,3] While the rigid backbones of the molecules provide stiffness, the aliphatic side chains render the molecules soluble in organic solvent, improve their transfer by LBK deposition, and provide a liquidlike matrix for the rods. Optimal exploitation of nanostructures using these molecules requires a good understanding of their arrangement in LBK multilayers, both as deposited and after subjection to elevated temperatures. In many cases of technological interest a fabricated structure must be stable to substantial temperature fluctuations.

Characterization of the bulk behavior of α-helical poly(L-glutamate) homopolymers[4–6] and copolymers[7–9] with flexible side chains, illustrated schematically in Figure 1 and with their chemical structure in Figure 2, has been undertaken by others, and these efforts suggest features which one might expect to see in the multilayers. Homopolymers having n-alkyl side chains with $n \geq 10$ exhibit side chain crystallization[4] and a resultant ordering into a layered structure with the crystalline aliphatic chains sandwiched between layers of peptide backbones. It has been suggested by Watanabe *et al.*[4] that the side chains from molecules in adjacent layers are significantly interdigitated, as shown schematically in Figure 3. However, this interdigitation has not been observed directly.

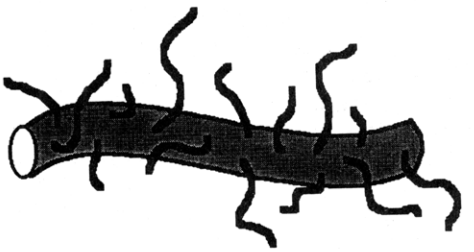

Figure 1. Schematic of a single molecule of a poly(L-glutamate) "hairy-rod" polymer.

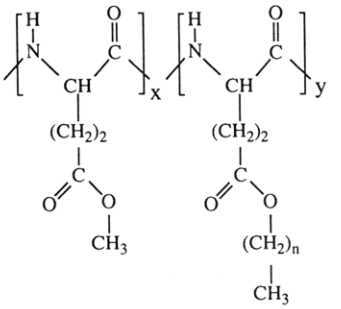

Figure 2. Chemical structure schematic of a family of poly(L-glutamate)s of interest in this work. The particular copolymer for which results are presented has $x = 0.7$, $y = 0.3$, and $n = 17$.

Figure 3. Interdigitated side chain structure of octadecyl-substituted poly(L-glutamate) in the bulk as proposed by Watanabe.[4]

The homopolymer most closely related to the copolymer studied in this work is that with $n = 17$ (see Figure 2).

* To whom correspondence should be addressed.

† Present address: Department of Chemistry, University of Arizona, Tucson, AZ 85721.

‡ Present address: BASF Aktiengesellschaft, Kunststofflaboratorium, 6700 Ludwigshafen, FRG.

§ Also with Frontier Research Program, The Institute of Physical and Chemical Research (RIKEN), Wako Saitama (Japan).

® Abstract published in *Advance ACS Abstracts,* October 1, 1994.

0024-9297/94/2227-6893$04.50/0

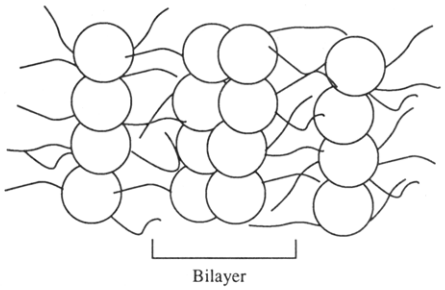

Figure 4. Schematic structure illustrating multilayers with backbones preferentially located at the center of each double layer. Circles represent the α-helical backbone including the methyl ester group.

When heated to 60 °C this homopolymer undergoes a first-order transition to a liquid crystalline phase with hexagonal symmetry.[6] The existence of this liquid crystalline phase suggests a means by which monodomains might be created in thin films of this or related materials. Behavior or related copolymers having both methyl- and *n*-alkyl-substituted residues depends on the degree of substitution with the *n*-alkyl side chain (see Figure 2). In particular, the side chains in polyglutamates with intermediate degrees of substitution are less likely to crystallize.[7] Tsujita *et al.*[9] report that copolymers with 16% octadecyl side chains (n = 17) do not display side chain crystallization while those with 52% or greater substitution do. This difference in side chain behavior also leads to a large increase in the interlayer spacing from 11.6 Å for 16% substitution to 28.8 Å at 52% substitution. While the distance between layers in the bulk has been studied with X-rays,[7,8] the spacing between rods within a layer remains a matter of conjecture. Calculations based on the density of the bulk material suggest that the spacing should be about 12.3 Å for the octadecyl-substituted homopolymer.

It is not intuitively clear how similar the structure of LBK deposited multilayers of polyglutamates may be to that of their bulk counterparts. However, it has been speculated that the interdigitation of the side chains could be significantly less prevalent in the as-deposited multilayers due to the nature of the fabrication process. The LBK technique is generally thought of schematically as providing multilayers through the stacking of discrete layers. However, it is unclear how the degree of side chain interdigitation might develop with time, or at elevated temperatures. Such interdigitation of parts of the molecules represents an important type of interlayer mixing which may occur on a scale smaller than that characteristic of the molecular center of mass diffusion among separate layers.

Experimental work using a variety of techniques has provided several clues to the structure and properties of PG copolymer LBK monolayers and multilayers[2,3,10] including information on the topology and stability of the surface.[11-13] These results are consistent with the schematic structure model shown in Figure 4, which envisions the multilayers as composed of double layers with the helical backbones located preferentially at the center of each double layer. The average double layer spacing for thick (ca. 300 layers) multilayers measured[2] with conventional small angle X-ray scattering is considerably smaller than that expected in the case where layers do not interdigitate. Also, atomic force microscopy (AFM) measurements of a bilayer of PG on a Si substrate indicate a thickness[13] which is larger than that seen in the multilayer, illustrating that when PG is next to a surface not allowing interdigitation, the bilayer thickness is greater. However, details of the layer structure, particularly the role of interdigitation of the side chains in adjacent layers, remain to be elucidated. In the present study neutron and X-ray reflectometry are combined to investigate this structure and its change upon annealing of the layers at elevated temperatures.

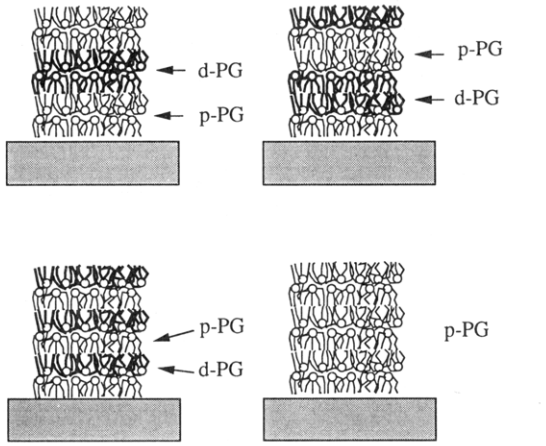

Figure 5. Schematic drawings of the various multilayer architectures used to aid the structure elucidation with neutrons (top left to bottom right): (a) ppdd; (b) pddp; (c) pdpd; (d) pppp.

Experimental Section

Materials. Poly[(γ-methyl-L-glutamate)-*co*-(γ-octadecyl-L-glutamate)] (PG), shown schematically in Figure 2, is a statistical copolymer of substituted glutamic acid repeat units. About 70% of these units have short methyl ester side chains, while about 30% have octadecyl chains replacing the methyl group. This ratio of short and long chains provides good LB transfer characteristics while avoiding the low-temperature side chain crystallization characteristic of more highly packed long chains. Both molecules with protonated side chains (p-PG) and partially deuterated side chains (d-PG) were prepared, the degree of deuteration in the second case being about 95%. The synthesis of p-PG has been described in ref 14, and that of d-PG in ref 15.

The structure of a single molecule of this "hairy-rod" polymer is shown schematically in Figure 1. At the temperatures considered in this work, the PG is known to be in an α-helical conformation, changing to a β sheet structure only when heated to temperatures above 412–433 K.[16] The α-helix has a pitch of 5.4 Å and diameter, d, of 5.6 Å with 3.6 monomer units in each revolution.[17] The average distance to which the methyl ester side chains extend from the peptide backbone, when measured as projected onto a plane perpendicular to the rod's axis, is about 4.3 Å. Thus, the diameter of the cylindrical volume including both the polypeptide backbone and the methyl ester side chains is about 14 Å. Light scattering measurements[15] of the p-PG in 0.5% solutions of $CHCl_3$/formamide indicate a molecular weight, M_w, of about 460 000, which corresponds to a degree of polymerization of about 2100 and a contour length, L, of the molecule of approximately 3200 Å.

Sample Preparation. In order to provide the greatest possible information on the structure of the multilayers, four types of samples, all shown schematically in Figure 5a–d, were studied. In the first three, layers containing only p-PG or only d-PG were deposited in a systematic way to provide contrast for neutron reflectometry at one type of interface. The fourth contained all p-PG layers and had a great many more layers than the other samples. The first sample type, shown in Figure 5a, contained molecules of the same type in both layers of each bilayer, but the molecule type was alternated between bilayers. Thus, the first two layers deposited were both of p-PG, the second two were of d-PG, and this pattern repeated seven times (for a total of 32 layers). As a designation for this sample architecture we adopted the shorthand notation "ppdd", suggesting a repeat structure of two protonated layers followed by two deuterated layers. In a similar way, the other three architectures were designated as "pddp", "pdpd", and "pppp". The total number of layers deposited in these structures were 24, 30, and 160, respectively.

Three multilayers were deposited on 76 × 50 × 0.5 mm³ rectangular substrates, while pppp was deposited on a 25 × 25 × 0.5 mm³ substrate, all cut from silicon wafers (provided by Wacker Chemical). The substrates were cleaned by ultrasonification, first in hot chloroform for 15 min and then in a hot 1:1:5 solution of $NH_4OH:H_2O_2:H_2O$ for 30 min. After rinsing in Millipore water, the surfaces were rendered hydrophobic by etching in an Ar/O_2 plasma (0.9 mbar/0.1 mbar) and then treating them with NH_4F. PG monolayers were prepared using a KSV 5000 alternating layer trough (KSV Instruments) in a clean room at BASF, Ludwigshafen, Germany. The molecules were spread from a 0.3 mg/mL solution in chloroform onto a Millipore-quality water subphase and compressed at 20 °C to a surface pressure of 20 mN/m before transfer. A Y-type deposition was performed using a dipping speed of approximately 20 mm/min. Transfer ratios (±0.05) for all but the first layers were between 0.9 and 1.0. With each sample the first layer transfer ratio was slightly lower than the rest. Annealing of the samples was done in a vacuum oven at roughly 100 mTorr. Samples were cooled to 4 °C except during measurements to avoid spurious annealing effects in the sample structure.

X-ray Reflectometry. X-ray reflectometry measurements were performed on three different reflectometers at the Max-Planck-Institut (MPIP), the National Institute for Standards and Technology (NIST), and the University of Akron (UA). All three use Cu K_α radiation (λ = 1.54 Å) and pyrolytic graphite monochromators. The MPIP reflectometer[18] is mounted on an 18 kW rotating anode source and uses comparatively long collimation and sample to detector distances to maximize attainable resolution for a given dynamic range. The NIST apparatus is mounted on a sealed tube and is very compact to achieve an excellent dynamic range with moderate resolution. Data obtained on the UA device were collected using a configuration which also provided a large dynamic range at the price of moderate resolution. All measurements, typically lasting several hours, were performed in air at room temperature.

Neutron Reflectometry. Measurements were performed on the fixed wavelength (λ = 2.35 Å) reflectometer on beam tube seven at the National Institute of Standards and Technology NBSR research reactor. The resolution of the wavelength was constant at about $\delta\lambda/\lambda = 0.015$, while the relative resolution of the incidence angle θ, $\delta\theta/\theta$, improved somewhat with θ, even though the collimating and detector slit sizes were increased gradually through the course of the measurement to maximize intensity. Overall the relative resolution of the incident wave vector component perpendicular to the surface, k ($=2\pi(\sin\theta)/\lambda$) varied from about 0.0009 at the critical value for total reflection to about 0.0029 at the largest values of k measured. All data sets were corrected for background and the effect of varying slit size before being analyzed. While a few measurements were performed at 4 °C in a temperature-controlled sample chamber, the majority were performed in air at ambient temperature.

Theory and Analysis Method

When a collimated beam of radiation strikes the surface of a flat sample at glancing incidence, some fraction of the radiation is reflected at a glancing angle equal to the angle of incidence. The ratio of the reflected to incident intensities is referred to as the reflectivity, and the variation of this ratio with incident angle is characteristic of features in the sample microstructure in the direction perpendicular to the sample surface. The microstructural variations to which the technique is sensitive are those resulting in modulation of the scattering length density, b/V, which is related the refractive index, n, for X-rays of neutrons by

$$n_x = 1 - (\lambda^2/2\pi)(b/V)_x \qquad n_n = 1-(\lambda^2/2\pi)(b/V)_n \quad (1)$$

For neutrons the contrast in the sample arises from differences in the neutron scattering cross sections of the various nuclei in the sample, principally hydrogen and deuterium, which have neutron scattering lengths, b_i, of -0.374×10^{-12} and 0.667×10^{-12} cm, respectively. Scattering length density is readily calculated by summing all isotopic scattering lengths in a representative repeat unit of material and dividing by the corresponding repeat volume.

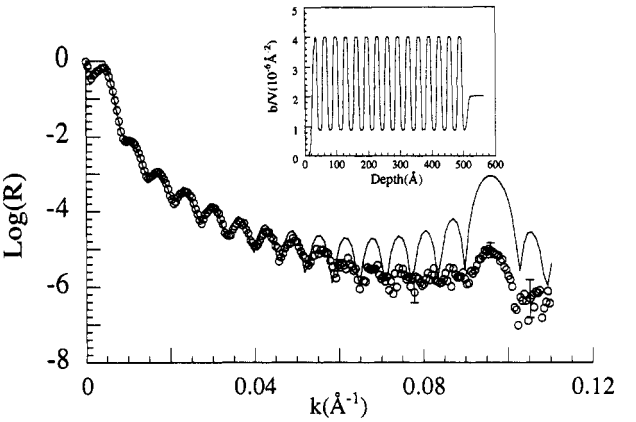

Figure 6. NR data for pdpd unannealed shown along with an unrealistic model curve based on the model $(b/V)_n$ profile in the inset, which assumes no interdigitation between layers exists.

For X-rays the basis for contrast is the difference in electron density between atoms. In this case, if one is far from an absorption edge, scattering strength may be assumed to be proportional to the number of electrons per atom, Z. The calculation for scattering length density is done by summing the total number of electrons available in a repeat unit, multiplying by the effective scattering length of a single electron, r_e, the classical Thomson electron radius, and accounting for mass density. The scattering length density varies in an orderly fashion through the periodic table for X-rays, while it varies nonuniformly for neutrons. Since the samples studied here contain several elements, the structural profiles will be reported in terms of the scattering length density rather than composition of a particular component. It should be kept in mind that regions displaying a larger value of $(b/V)_n$ generally contain a higher fraction of deuterated material.

Figure 6 presents a semilogarithmic plot of neutron reflectivity as a function of k for the sample designated pdpd. This and other reflectivity figures include statistical error bars for selected points to help visualize the uncertainty of the data points. Three key features of the data are apparent even without any detailed analysis. First of these is a well-defined value of k at which the reflected intensity falls off dramatically from a value near unity. This critical value, k_c, is characteristic of the scattering length density of the most highly reflective material in the sample, be it the deuterated organic material or the substrate. The second of the three outstanding features is the interference pattern consisting of many local maxima and minima in the curve. These fringes, sometimes referred to as "Kiessig fringes",[19] are indicative of the sample's overall thickness and their frequency increases with increasing sample thickness. The third of the three features we note is a peak at k^* near the maximum value of k studied. This Bragg peak, analogous to those seen in wide angle diffraction patterns of crystalline systems, arises from a periodic spacing, D, of uniform domains oriented parallel to the sample surface. Its position, k^*, is related to D by

$$D = \pi/k^*_{true} \qquad k^*_{true} = (k^*_{apparent}{}^2 - k_c{}^2)^{1/2} \quad (2)$$

As with all scattering techniques, the detailed analysis of X-ray and neutron reflectivity data presents us with a certain ambiguity due to a loss of phase information. It is impossible to derive a unique model of the structure solely from the experimental scattering data. Instead, we seek a model, consistent with all that we know of the system from other means, that is sufficiently complex to capture all the observed features. Also important in the development of the model is the criterion that it must reconcile X-ray reflectivity data from the same sample as well.

In the present case it is apparent that the data justify a model incorporating, at the least, a specific value of overall average scattering length density, a particular overall thickness, and one characteristic spacing. Reconciling the present data will further require specifying the microroughnesses of interfaces across which $(b/V)_n$ varies significantly. Roughly stated, the magnitudes of these roughnesses manifest themselves in the overall level of reflectivity, the rapidity with which the reflectivity falls with increasing k, and the amplitude of the Kiessig fringes. For the purposes of presenting the data analysis we will adopt a hierarchical approach, considering first the simplest possible model and then adding detail as necessary to capture all features of the curve. An attractive feature of this approach is that it illustrates how certain parameters can, in fact, be inferred nearly independently of others.

The best parameter values for a given model are determined from the data by means of regression. Since this regression is highly nonlinear and often does not readily converge when fully automated, several iterations are made interactively by the researcher, and one resorts to an automated procedure only once the parameter values have been well constrained. The calculation of the reflectivity proper is done using an optical matrix formalism.[20] In this method the reflection (and transmission) properties of a uniform layer i of scattering length density b/V and thickness d_i are determined from a 2×2 transform matrix, $\mathbf{M}$, of complex elements which depend on b/V and k_z[20]

$$\mathbf{M} = \begin{pmatrix} \cos(k_{z,i}d_i) & -\sin(k_{z,i}d_i)/k_{z,i} \\ k_{z,i}\sin(k_{z,i}d_i) & \cos(k_{z,i}d_i) \end{pmatrix} \quad (3)$$

$$k_{z,i} = [k_z^2 - 4\pi(b/V)_i]^{1/2} \quad (4)$$

where $k_{z,i}$ is the magnitude of the z component of the refracted beam's wave vector in the layer. The reflectance (the amplitude of the reflected wave) from this layer is given by

$$r_{i,i+1} = (k_{z,i} - k_{z,i+1})/(k_{z,i} + k_{z,i+1}) \quad (5)$$

and the reflectivity by the product of the reflectance and its complex conjugate. By appropriate substitution for b/V and k this same formalism may be used for both X-ray and neutron reflectometry, though its physical interpretation differs for the two techniques.

In order to simulate the reflectivity for nonuniform model composition profiles, the matrix formalism is simply extended by discretizing the continuous profile using sufficiently small steps.[21] Each step is then associated with a fictitious sublayer of uniform scattering length density and a corresponding optical matrix. The effective transform matrix for the entire profile is found as the product of all the sublayer matrices. Interface microroughness is thus readily incorporated by approximating the profile at a rough interface as a diffuse continuous one with a width co rresponding to the degree of microroughness. For the conditions studied here an appropriate approximation envisions the interfaces as having random roughness with Gaussian distributions of height, corresponding to an error function type interfacial profile.[22]

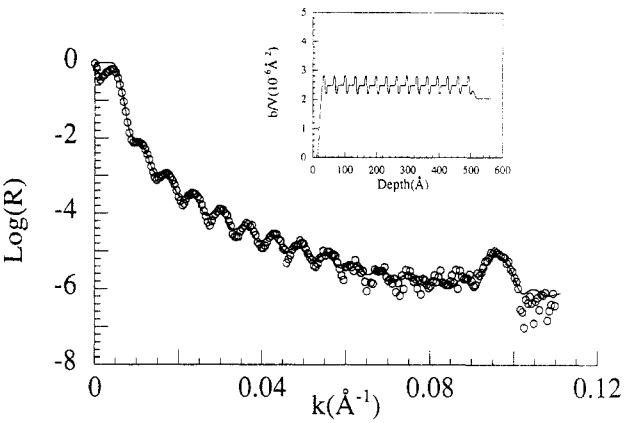

Figure 7. NR data for pdpd as deposited shown with a simulated curve which matches the curve reasonably well but corresponds to the unrealistic profile shown in the inset.

We demonstrate the analysis in some detail for one sample. That portion of the pdpd neutron reflectivity curve for $k < k^*$ may be fit first using a model consisting only of a uniform film of thickness 490 ± 5 Å, average scattering length density 2.48×10^{-6} Å^{-2}, and microroughnesses of 6 ± 3 Å rms (root mean square) for the air/polymer interface and 8 ± 6 Å rms for the polymer silicon interface. This air/polymer interface roughness corresponds well to the value of 7 ± 2 Å rms reported using AFM.[13] In general, NR and XR can be very sensitive to the overall film thickness. In the present case, however, the average $(b/V)_n$ of the film is nearly equal to the $(b/V)_n$ of the substrate and the sensitivity is not as good for neutrons as it is for X-rays. The reflectivity curve is always most sensitive to those features associated with the largest jumps in (b/V).

The next step in the analysis is to include an additional feature in the model which is capable of producing the observed Bragg peak. In Figure 6 is shown the $(b/V)_n$ profile for a model which assigns the theoretical $(b/V)_n$ value of pure p-PG or d-PG to each of a model multilayer's 30 component layers and incorporates some microroughness at every interface. Also shown is a comparison between the neutron reflectivity expected for such a model and the pdpd experimental data. The position of the experimental Bragg peak is represented well when a bilayer thickness of 32.7 ± 0.5 Å is used. However, the proposed model exhibits a much larger Bragg peak than does the sample. Broadening of the interfaces between the regions of higher and lower $(b/V)_n$ reduces the height of the Bragg peak but is insufficient to match the experimental data. Thus one must conclude that either additional features or a reduced $(b/V)_n$ modulation amplitude, $\Delta(b/V)_n = (b/V)_i - (b/V)_i - (b/V)_{i+1}$ is needed for the model.

The height of the model Bragg peak depends on the degree to which the model multilayer $(b/V)_n$ profile varies above and below its overall average value. Reducing the area between the multilayer profile and the line of constant $(b/V)_n$ equal to $(b/V)_{av}$ reduces the Bragg peak magnitude. Unfortunately, the shape and magnitude of the first-order Bragg peak is not particularly sensitive to the detailed distribution of the scattering length density about the average, so long as the profile is periodic and has the proper characteristic repeat spacing. To emphasize this point, two rather different profiles which yield comparable fits to the data are shown in the insets of Figure 7 and 8.

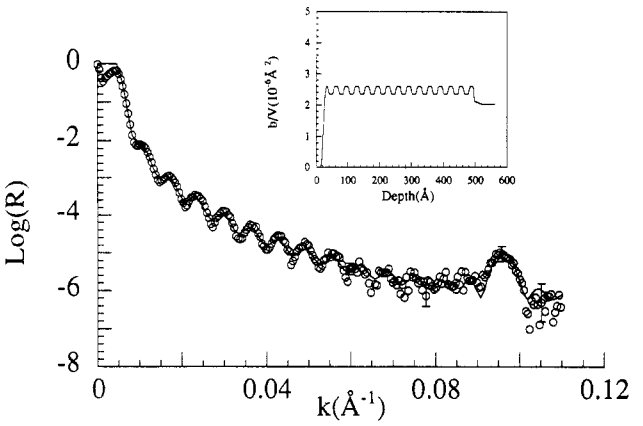

Figure 8. NR data for pdpd as deposited with a model curve corresponding to the profile in the inset and the parameters summarized in Table 1. Properly accounting for interdigitation yields an excellent representation of the data.

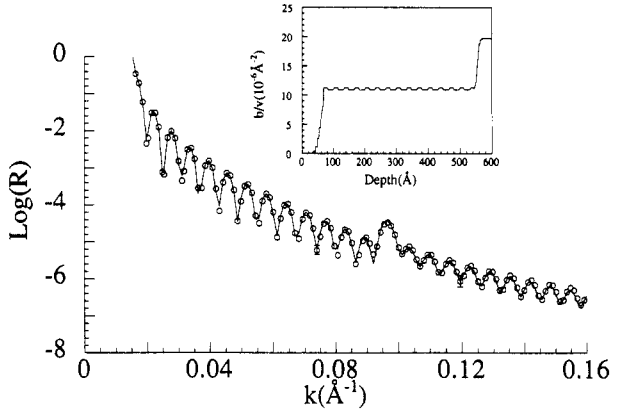

Figure 9. Rigorous test of the structural model proposed for pdpd as deposited, where the XR data are compared to a model X-ray reflectivity curve derived from the identical structure model used to fit the NR data in Figure 8. The $(b/V)_x$ profile is shown in the insert.

Discriminating between the two models on the basis of NR alone requires data at higher values of k, as demonstrated below with other data sets. However, our understanding of the molecules' chemical structures suggest some reasonable limits to the dimensions of various regions in the model. For example, the existence of a sharply defined, 2.5 Å wide region of very large $(b/V)_n$ in the model above seems unrealistic. A model with regions having dimensions comparable to those of a single layer or part of a molecule (e.g. the backbone diameter) cannot have such a large difference between the regions' scattering length densities. This smaller modulation is consistent with some type of overlap among the layers. The amount and type of possible overlap is considered in the discussion below.

In order to further constrain the analysis of the data, one should consider the X-ray reflectivity of this sample, shown in Figure 9, as well. If one estimates the $(b/V)_x$ values expected for bulk regions of the two types of PG, one finds a negligible difference. In fact, the X-ray reflectivity expected from the present model, which differentiates only between layers of different types, but not between different portions of one layer, is incapable of explaining the observed weak Bragg peak. Very good agreement is found with the overall sample thickness and roughnesses used to fit the neutron data, confirming those values. However, some modulation of $(b/V)_x$ must be included in a model to quantitatively fit the X-ray data. This could be due, for instance, to intralayer structure. An outstanding representation of the data, shown in Figure

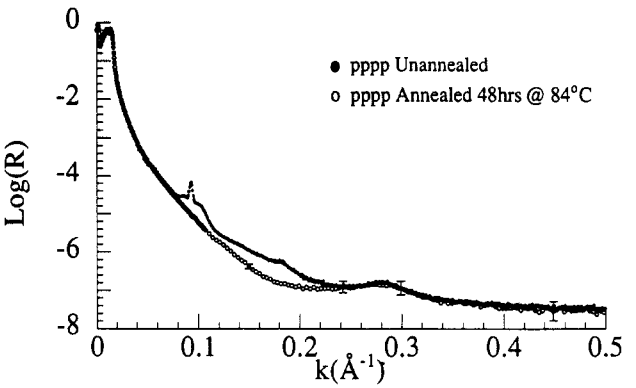

Figure 10. XR data for pppp as deposited and after annealing at 84 °C for 48 h. The presence of the second-order peak initially indicates that the modulation of $(b/V)_x$ is not perfectly symmetric.

9, may be obtained by adopting a model with about a 5% modulation in $(b/V)_x$. The maximum possible modulation is constrained in this case by the fact that the intrinsic contrast between the materials of the film is limited. On the other hand, with only one Bragg peak in the data one is not strongly sensitive to dimensions of the regions of higher and lower $(b/V)_x$, only to the period of the modulation. When a second peak is present, as for the pddp sample discussed below, these further dimensions may be precisely ascertained.

The spacing indicated by the X-ray Bragg peak position, 33.1 ± 0.25 Å, corresponds reasonably well to the thickness of two layers one deduces from the neutron data, and the overall multilayer thickness is the same as well. This consistency strengthens our confidence in these fundamental parameter values and underscores the advantage of using neutron and X-ray reflectometry as complementary probes. An even more striking aspect of this complementarity, however, is the fact that X-rays uniquely provide detail of the *intra*layer structure while neutrons are uniquely sensitive to the *inter*layer interfaces.

Results and Discussion

As-Deposited Multilayers. Samples of all four types described above were studied with X-rays and three with neutron reflectometry in hopes of providing the greatest possible number of constraints in building a structural model for the multilayers. In order to be a valid possibility, the characteristic features of a candidate model had to be consistent with data from all four sample types. The neutron contrast between protonated and deuterated side chains is about twice that between the backbones and side chains of a given layer. Thus, in the ppdd sample, the sample feature which should dominate the measured neutron reflectivity, in the range of k probed, is the scattering length density profile at the interfaces between protonated chains belonging to one bilayer and the deuterated side chains belonging to another bilayer, as seen in the ppdd picture in Figure 5a. In the pddp sample the interface profile between layers of the same bilayer is highlighted and in the pdpd sample interfacial profiles of both types will figure importantly in the measured reflectivity, as seen in Figure 5b,c, respectively.

We consider first the sample containing only one type of layer. X-ray data for pppp, shown in Figure 10, were obtained at moderate resolution over a rather large range of k. Clearly observable are three peaks corresponding to nominal spacings of 34.4 ± 0.1, 17.2 ± 0.1, and 11.1 ± 0.3 Å, as listed in Table 2. These data are less amenable to quantitative representation by a model curve than are those from the other, thinner samples. This is most

Table 1. Structure Parameters from Neutron Reflectometry[a]

	anneal		overall thickness,	single layer thickness, Å		$10^6(b/V)$n, Å^{-2}				roughness Å rms		p-PG/d-PG interface
	temp, °C (±1.5	time, h (±0.15)	Å (±5)	d-PG (±0.25)	p-PG (±0.25)	d-PG layer	p-PG layer	av	Δ	air/PG (±3)	PG/glass (±6)	width, Å rms (±2)
theory						4.3 ± 0.2	0.93 ± 0.05	2.6 ± 0.1	3.37 ± 0.2			
pdpd	as deposited		490	15.9	16.8	2.60 ± 0.05	2.35 ± 0.05	2.5 ± 0.3	0.25 ± 0.05	6	8	3
	70	4	–[b]	–	–	–	–	–	–	–	–	–
ppdd	as deposited		540	16.2	16.9	3.20 ± 0.15	1.25 ± 0.15	2.2 ± 0.3	1.9 ± 0.15	10	3	8
	70	5	–	–	–	–	–	–	–	–	–	–
pddp	as deposited		394	16.3	17.0	3.50 ± 0.15	1.5 ± 0.15	2.5 ± 0.3	2.0 ± 0.15	8	8	3
	84	4	–	–	–	–	–	–	–	–	–	–

[a] Where given at the top of a column, estimates of error for parameter values from experimental data are uniform throughout the column. [b] – denotes no change from previous measurement.

Table 2. Structure Parameters from X-ray Reflectometry[a]

experimental conditions anneal			qualitative observations peaks present[b]			model parameter estimates								
sample	temp, °C (±1.5)	time hour (±0.15)	1st	2nd	3rd	overall thickness, Å (±5)	spacing D, Å (±0.2)	$10^6(b/V)_x$, Å^{-2} av	$10^6(b/V)_x$, Å^{-2} Δ (±0.05)	roughness, Å (rms) air/PG (±3)	roughness, Å (rms) PG/glass (±2)	interface width, Å (±1)	high b/V region width, Å	low b/V region width, Å
limits								10.6	2.8					
pppp	as deposited		Y	Y	Y	NA[c]	34.4	10.2 ± 1	0.4	6	7	2.4	19.9 ± 1	14.5 ± 1
	84	4	N	N	Y	NA	–	–	–	–	–	–	–	–
	84	167	N	N	Y	NA	–	–	–	–	–	–	–	–
pdpd	as deposited		Y	NA	NA	497	33.1	11 ± 1	0.4	10	6	2.4	16.5 ± 3.5	16.5 ± 3.5
	70	4	Y*	Y	Y	487	32.5	11 ± 1	0.2	11	14	2.4	19.5 ± 1	13.1 ± 1
	84	4	Y	Y	Y	–	–	–	–	–	–	–	–	–
	84	67	Y	Y	Y	–	–	–	–	–	10	–	–	–
ppdd	as deposited		Y	NA	NA	535	33.3	11 ± 1	0.4	11	6	2.4		
	70	5	Y	Y	Y	525	32.8	11 ± 1	0.2	10	7	2.4		
pddp	as deposited		Y	Y	Y	401	33.45	10.2 ± 0.3	0.4	8	9	2.4		
	84	4	Y*	Y	Y	396	33.1	11.0 ± 0.5	0.2	8	9	2.4	19.8 ± 1	13.3 ± 1

[a] Where given at the top of a column, estimates of error for parameter values from experimental data are uniform throughout the column. [b] "Y" = present, "N" = missing, "Y*" = present but reduced in intensity from previous measurement. [c] NA denotes not available. [d] "–" denotes no change from previous measurement.

probably due to a greater variance of layer to layer structure in the thicker sample. However, two qualitative results are available which prove important for comparison with the other sample types. First, the presence of a second-order peak indicates that the variation in $(b/V)_x$ is not perfectly symmetric, i.e. the regions of above average $(b/V)_x$ are of a different thickness than those of below average $(b/V)_x$. Second, a feature of average dimension 11.1 Å is present in the sample. The breadth of the third peak suggests that this periodicity is not well-defined. However, the precise character of this feature is still not understood.

Results for the pdpd sample are displayed in Figures 6–9 and were discussed in part in the above illustration of the analysis technique. Model structure parameter estimates corresponding to best fits to the data are summarized in Tables 1 and 2. While the goodness of fit to the NR data is very sensitive to the amplitude of scattering length density modulation, $\Delta(b/V)_n$, used, it is less sensitive to the absolute values of $(b/V)_n$ used for the two layer types. Even so, one may compare the experimental values with calculated neutron scattering length densities for pure p-PG and d-PG (95% deuterated) shown in Table 1. These are calculated using elemental compositions estimated from NMR and volumes per repeat unit derived from monolayer studies ($\rho_{p\text{-}PG} = 1.154$ g/cm^3, $\rho_{d\text{-}PG} \geq \rho_{p\text{-}PG}$) and represent limiting values. The $(b/V)_n$ values measured with NR for d-PG and p-PG using a multilayer of d-PG atop a multilayer of p-PG,[19] where the values are expected to attain nearly their bulk magnitudes, are ca. 4.3×10^{-6} and 1.2×10^{-6} Å^{-2}, respectively. The sample average $(b/V)_n$ reported for the present reflectivity data is about 4% less than that calculated from theoretical pure component values and also less than that from the two part multilayer of ref 23. However, these differences lie within the error estimates associated with these parameter values. Differences in this range could also be due to errors from the determination of the transfer ratios during deposition.

The X-ray results show that the polypeptide backbones are located preferentially near the center of each bilayer, reflecting the asymmetry of the original monolayers formed on the water surface prior to transfer. There the hydrophilic backbones lie on the water and aliphatic chains project into the air. When transferred to the substrate using a Y-type transfer, the backbones of layers within the same bilayer are placed close together. In Table 2 the film's average $(b/V)_x$ and amplitude of X-ray scattering length density modulation, $\Delta(b/V)_x$, are compared with limiting values calculated by assuming a fictitious structure with layers containing only backbones and layers containing only amorphous aliphatic chains. Reflectivity is a sensitive probe of the $(b/V)_x$ modulation, as indicated by the errors assigned to $\Delta(b/V)_x$. However, it is not as sensitive to the absolute magnitude of $(b/V)_x$. The observed $(b/V)_x$ modulation is much less than the limiting value, suggesting that even in the regions containing the backbones, many side chain portions are present as well. Also, any tilt of the these long rods is a factor reducing the $(b/V)_x$ modulation. A crude sketch suggesting how this might appear is presented in Figure 4. Calculations of the diameter of the electron rich cylindrical region containing both the backbone and methyl ester moieties of a single polyglutamate molecules provide a value of about 14 Å.[24] Without the inclusion of the ester moieties, the diameter is about 6 Å. As seen in Table 2 the width of the electron rich hig h$(b/V)_x$ region is about 19 Å, depending on the sample. Figure 11 illustrates a model accommodating this value by allowing interpenetration of the α-helical back-

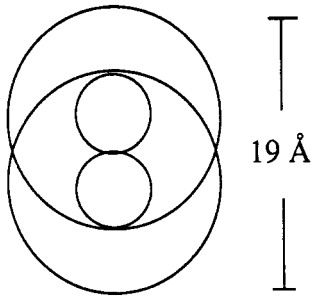

Figure 11. Schematic illustrating how the ester moieties of adjacent α-helix backbones may overlap.

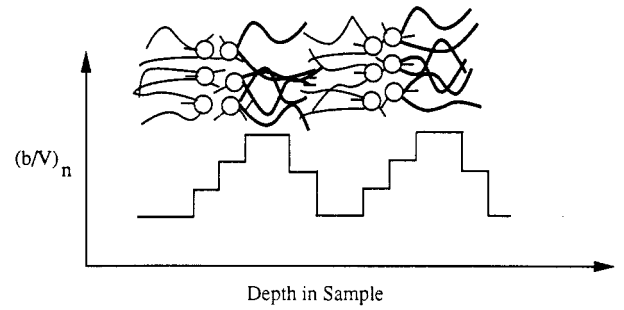

Figure 12. Schematic of an idealized multilayer structure and the corresponding neutron scattering length density profile.

bone through the space occupied by the methyl ester moieties. This interpenetrating model has been corroborated using molecular modeling simulations,[24] which suggest that for noninterdigitating layers the greatest possible width for a region containing only long side chains would be ca. 14 Å (e.g. 7 Å for each of two adjacent layers if there were no interdigitation of the side chains).

The comparatively small difference between the $(b/V)_n$ experimental values of the what are nominally the p-PG and d-PG layers indicate unquestionably that there is some type of mixing of the two molecule types. Two possible mechanisms for this mixing are interdigitation and molecular interchange of center of mass diffusion between layers. Analysis of the unannealed sample data alone cannot distinguish between these two mechanisms. However, the lack of change upon annealing, discussed below, strongly argues in favor of interdigitation. Quantifying the amount of interdigitation is thus an important issue. This problem may be discussed with the help of the schematic structure and corresponding neutron scattering length density profile in Figure 12. The side chains for each rod are depicted as lying perferentially on one side of the rod, as dictated by the geometry of the deposition procedure and the X-ray results, indicating the localization of rods to the interior of a given bilayer. As drawn, the model has five regions of distinct composition. Moving from left to right in Figure 12, we find protonated side chains only, backbones with protonated side chains, backbones with deuterated chains, deuterated chains only, and a mixture of deuterated and protonated side chains. One recognizes, in fact, that it is impossible to imagine any amount of interdigitation of this type which leads to a $(b/V)_n$ profile containing only two characteristic scattering length densities, unless the layers are so highly intermixed that the only distinction which remains is the existence of regions rich in backbones and regions rich in side chains. A variety of profiles containing detail such as that suggested in Figure 12 approximate the NR data as well as our simpler model, but none is superior. For greater sensitivity one must have data at larger k.

A comparison of model curves and the data does offer the following limitations on potential models. The greatest

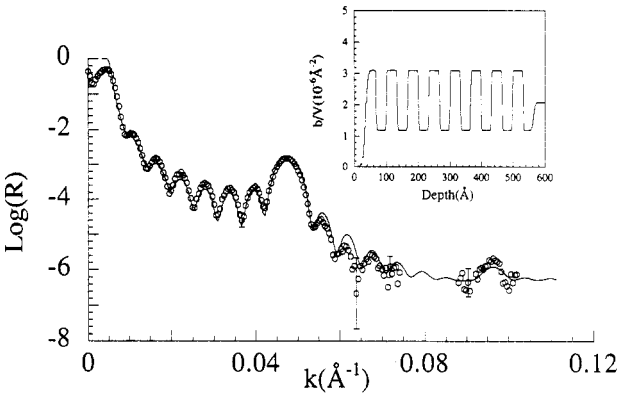

Figure 13. NR data for as-deposited ppdd together with a model curve corresponding to parameters in Table 1 and the profile in the inset. The existence of the second-order Bragg peak suggests the bilayers of protonated and deuterated material do not have identical thicknesses.

difference between the $(b/V)_n$ values of any regions in the multilayer structure cannot exceed about 0.8×10^{-6} Å^{-2}. Using an appropriate layer thicknesses, $(b/V)_n$ differences greater than this produce a Bragg peak which is too intense. Thus, barring molecular interchange between layers, no region rich in side chains can contain more than about 65% side chains of one type. This value is obtained by simply determining the deuterated to protonated ratio required to obtain the $(b/V)_n$ difference. All in all, the picture of the pdpd structure which emerges is one of extensive interdigitation.

Figure 13 displays neutron reflectivity data for ppdd. For this sample the technique should be sensitive only to interfaces and dimensions of bilayers and not to those of individual layers. Indeed, the value of k at the first Bragg peak maximum, k^*, is observed to be roughly half that for the pdpd sample. This position reflects a bilayer spacing of 33.1 ± 0.3 Å. Due to time constraints, reflectivities were not collected for the entire range of k studied for the pdpd sample. However, the neighborhood about $k = 2k^*$ has been probed in order to confirm the presence of a weak second-order Bragg peak. A precise characterization of the Bragg peak's relative intensity is difficult because the measurement of the reflectivity for $k > 2k^*$ is limited. In any case, the existence of a weak second-order peak alone indicates that the dimensions of the protonated and deuterated bilayers are not identical. If they were, the second-order peak would not appear. A slight difference of 0.7 Å in the thicknesses of the two layer types has, in fact, been incorporated in the final model fit.

Using arguments similar to those presented above for the pdpd sample, one may obtain a simple two region periodic model structure sufficient to represent the ppdd data reasonably well. The corresponding model reflectivity curve and profile are portrayed in Figure 8. As summarized in Table 1, the bilayer spacing used is nearly the same as that for pdpd, and the average b/V for the entire multilayer is also similar. A feature of the profile of particular interest is the amplitude $\Delta(b/V)_n$ of the scattering length density variations. For this sample the amplitude is $(1.9 \pm 0.15) \times 10^{-6}$ Å^{-2}, much higher than the amplitude of 0.25 ± 0.5 Å^{-2} for the pdpd sample. The number of interfaces between p and d layers has been halved, but the amplitude of modulation $\Delta(b/V)_n$ has been increased by nearly a factor of 8. The type of interface which has been removed is that within the bilayer at which the backbones of p-PG and d-PG are closest. Since removing this interface increased $\Delta(b/V)_n$ so much, it seems that this type of interface contributes markedly to the mixing in the sample.

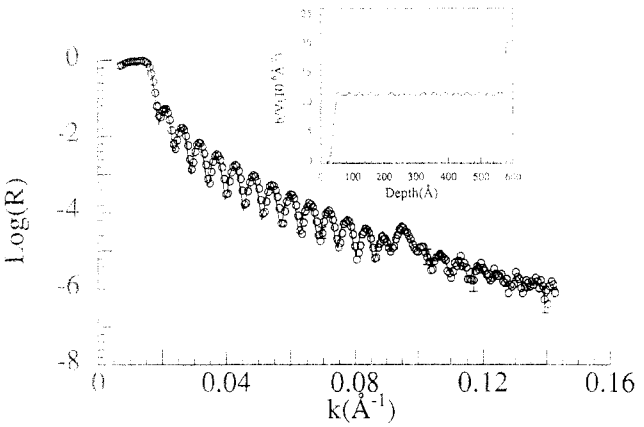

Figure 14. XR data for as-deposited ppdd with a model curve and the corresponding profile. The corresponding model parameters summarized in Table 2 agree well with those derived from neutron measurements.

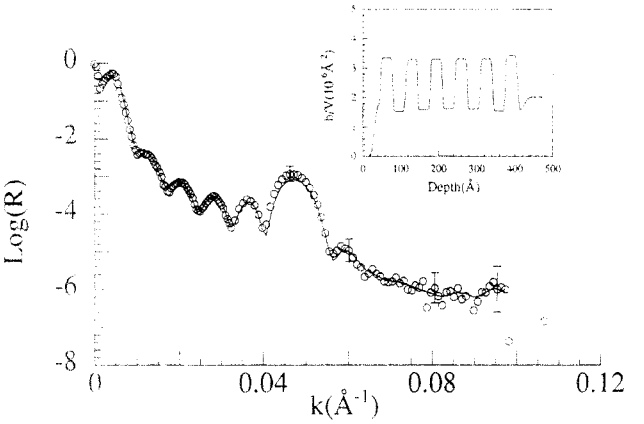

Figure 15. NR data for as-deposited pddp with a model curve and the corresponding profile in the inset. Model parameters are given in Table 1.

The significance of the microroughness values for bilayer/bilayer interfaces is limited. At best it provides only a gross indicator of the diffuseness of the interfaces, as NR cannot distinguish between smooth, laterally uniform changes in $(b/V)_n$ across the interface and abrupt, laterally nonuniform changes. Also, the microroughnesses are positively correlated somewhat with the magnitude of $\Delta(b/V)_n$.

X-ray data for ppdd are shown in Figure 14. Once again, the subdivision of each monolayer into two regions of differing $(b/V)_x$ is essential to adequately represent the reflectivity. The bilayer spacings, average $(b/V)_x$, $\Delta(b/V)_x$, and microroughnesses determined from these data, shown in Table 2, agree reasonably well with those from the pdpd sample. Agreement of the overall thicknesses, bilayer spacings, and roughnesses with those from the neutron experiment is also good.

Neutron data from the fourth sample to be considered, pddp, are presented in Figure 15. A strong first-order Bragg peak and weak second-order peak are observable, reinforcing the picture that the deuterated and protonated layers are slightly different in thickness. Layer thicknesses corresponding to the fit shown are consistent with those from the pdpd and ppdd samples. Interestingly, the amplitude of the scattering length density modulations for this sample is about the same as that for the ppdd sample. In contrast to the ppdd sample, where interdigitation of deuterated and protonated side chains is easily envisioned, here mixing of the two chain types can only occur readily in the neighborhood of the peptide backbones. The fact that $\Delta(b/V)_n$ is no bigger in this case than

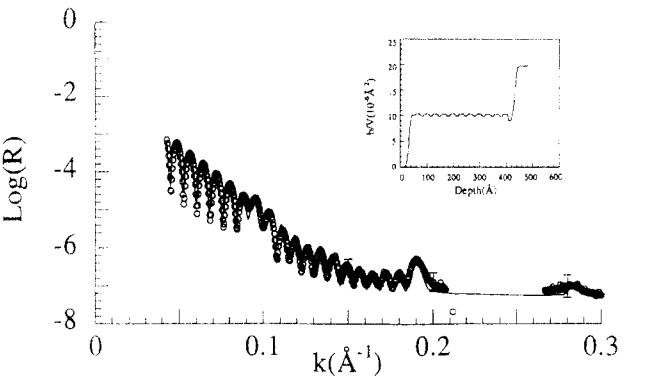

Figure 16. XR data for as-deposited pddp with a model curve corresponding to the profile in the inset and parameters in Table 2.

in the case where interdigitation of deuterated and protonated long side chains is easier suggests that either the lowering of contrast is due to mixing of entire molecules between layers or that interdigitation of long chains near the backbones is of great importance. The average $(b/V)_n$ is somewhat higher than that of ppdd and comparable to that of pdpd.

X-ray data for pddp as deposited, shown in Figure 16, is available over a somewhat larger range of k than for either pdpd or ppdd. This range affords the opportunity to observe a clear peak at a position corresponding closely to that expected for a second-order Bragg peak as well as a third-order peak. The existence of the second Bragg peak greatly narrows the possible models which can fit the data, as it allows one to specify to within ±1 Å the dimensions of the regions of higher and lower $(b/V)_x$. In particular, the region of above average $(b/V)_x$ has a thickness of 19.8 ± 1 Å and that of below average $(b/V)_x$ a thickness of 13.3 ± 1 Å. The region rich in backbones thus is certainly thick enough (i.e. >11 Å) to accommodate the polypeptide residues from each layer of a given bilayer, but not so thick (i.e. <28 Å) as to include both the polypeptides *and* all the methyl ester side chains of both backbones. Rather, the dimension of 19.8 Å corresponds well to the sum of the two polypeptide diameters and twice the average length of the short side chains. In contrast to the pdpd XR data the fit here is also very sensitive to the combination of regions used in the model. For example, it is not possible to place a slight dip in the $(b/V)_x$ profile between two regions of raised density to correspond to slightly separated rods. Thus, as also seen with the pdpd sample, the rods must be close enough together that the backbones and interdigitated methyl ester side chains are contained in a single region of nearly constant (b/V). This argues in favor of some crossing of the long side chains at this interface within the bilayer's interior.

Due to the particular thickness of this sample the goodness of fit is also very sensitive to the absolute value of $(b/V)_x$ for the first layer next to the substrate. Our analysis reveals that this value must be lower than those for any other layer and indeed examination of the transfer ratios show that the ratio for this first layer was somewhat poorer (82 ± 5%) than that for the others.

One may ask how reasonable it is from a thermodynamic point of view for the deuterated and protonated side chains to interdigitate. Studies of isotopic polymer blends[25,26] have confirmed that a small positive segment interaction energy exists between chains differing only in the substitution of D for H. This interaction has been ascribed[27-29] to the small changes in segment volume and polarizability associated with the exchange of D for H. The effect is so subtle, however, that it manifests itself in the form of a

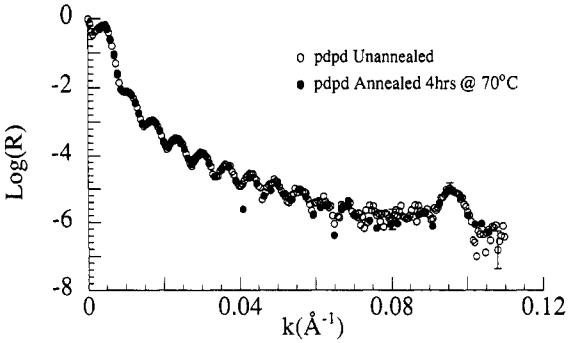

Figure 17. Comparison of the NR data for pdpd before and after an annealing of 4 h at 70 °C indicating no change in the interlayer structure.

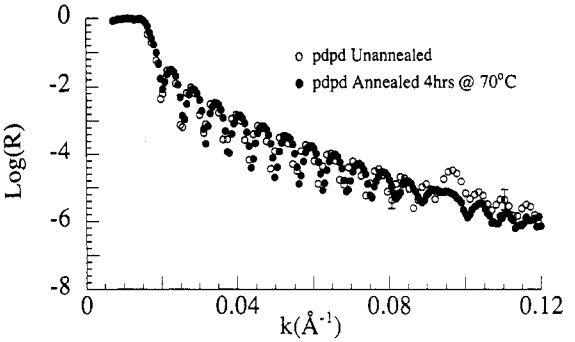

Figure 18. Comparison of the XR data for pdpd before and after annealing for 4 h at 70 °C revealing a relaxation of the deposition-induced intralayer asymmetry.

measurable upper critical solution temperature only for chain lengths greater than 10^3–10^4. Results of investigations by various groups[30,31] of *n*-alkane/*n*-deuterioalkane mixtures for *n* up to 40 are consistent with this view. Therefore, while the protonated and deuterated side chains are not perfectly equivalent, we do not expect any significant thermodynamic barrier to their mixing at all concentrations.

Annealed Samples. In further measurements the stability of the as-deposited structure to annealing was studied. Initially, samples were annealed at 70 or 84 °C for 4 or 5 h and then studied again with both X-rays and neutrons. Measurements were also done after still longer annealing treatments for pppp and pdpd. The exact annealing conditions are summarized in Table 2. In every case, the initial annealing had no discernible effect on the sample's neutron reflectivity over the range of *k* probed, as demonstrated in Figure 17 for the case of the pdpd sample. It follows that structural relationships among the different layers remained the same at the level of resolution afforded by the available *k* range. This result precludes the possibility of substantial center of mass diffusion of the molecules during this mild annealing treatment and is consistent with the results of the single interface study in ref 23. It is therefore highly unlikely that substantial diffusion took place at 4 °C from the time of deposition to the measurement of the unannealed samples (about 3 weeks). Only the deposition process itself remains as a possible opportunity when interlayer diffusion may have taken place. It is not known how the mobility of the molecules may have been affected while submerged in the aqueous subphase, but because PG is not soluble in water, no intermixing is expected. However, even in that condition any center of mass movement would have had to be highly cooperative, due to the rigid rod backbones,[32] and seems unlikely.

Another feature of the layer structure which is important in this regard is the degree to which the orientation of the rods in one layer corresponds to that in the next. For the larger samples, the flow of molecules onto the substrate during deposition is not convergent. Thus, one anticipates that orientation of the rods in neighboring layers will differ. This lack of orientation certainly hinders diffusion. The pppp sample is considerably smaller and the alignment of the rods between layers apparently is better in this case.[33]

Three types of changes with initial annealing were observed in the X-ray reflectivity in each case. First, the intensity of the X-ray first-order Bragg peak decreased markedly with annealing. An example of this change is shown in Figure 18 for the pdpd sample. Only the initial anneal of 4 h at 84 °C was required to fully eliminate the first peak in the X-ray reflectivity of pppp, but at least some hint of this peak remained after initial annealing of the other three samples. A structural model change which can represent this change in reflectivity is a reduction in the scattering length density modulation amplitude of a perfectly periodic structure. (That is, we allow no variation of layer thickness for layers of a given type.) Such a reduction may be rationalized by considering a delocalization of the peptide backbone positions, i.e. a relaxation of the intralayer asymmetry imposed by sample deposition. Such a relaxation seems plausible, since at elevated temperature the molecules have greater mobility and the configurational entropy gained by randomizing the positions of the backbones would easily offset any enthalpic costs due to changes in contacts. However, the thicknesses of the higher and lower (b/V) regions in the models used to fit the pddp XR data before and after annealing are essentially identical. This argues against a broadening of the spatial distribution of backbone axes in each bilayer with annealing.

Two additional changes seen in the structure of every sample are small decreases in the overall sample thicknesses and corresponding bilayer thicknesses. The observed decreases in sample thickness amount to about 10, 10, and 5 Å for the pdpd, ppdd, and pddp samples, respectively. Resolution in the XR for the thicker pppp sample was insufficient to measure its overall thickness change with annealing.

One feature which appeared to remain relatively unaffected by the annealing was the third broad peak shown in Figure 10. This constancy was observed directly for pppp and pddp, for which measurements were made out to at least a *k* of 0.5 Å^{-1} both before and after annealing. In fact, in the case of pppp, the third peak remained essentially unchanged after 6 days of 84 °C annealing. The third peak was also observed for pdpd, though first after an initial annealing of 4 h at 70 °C. Remarkable about this lack of change is the fact that the first- and second-order peaks both changed with annealing for the pppp and pddp samples. Four hours at 84 °C was sufficient to erase all signs of both the first- and second-order peaks from pppp, while the second-order peak from pddp was diminished but remained after the same treatment. A second-order peak was also present for the pdpd sample after 4 h at 70 °C and remained after an additional 67 h at 84 °C. Perhaps the second-order XR peak reflects the slight difference between the p and d layers as well as bilayer periodicity.

It was of particular interest to note after annealing of the samples if a hexagonal phase had been formed, as is seen in bulk samples of the octadecyl-substituted polyglutamate homopolymer and other rigid rod polymers such as polysilanes.[34] If a hexagonal phase had developed, one would have expected the appearance of a peak $k^* \cong 0.094$ Å^{-1} corresponding to the 100 spacing of about 34 Å. No

peak was observed at this position for any of the annealed samples. The fact that vestiges of the sample's multilayered character persist after annealing, even through extensive interdigitation occurs, could very vwell be due to the difference in rod alignment from layer to layer which hampers development of the alignment needed to form a 3-D ordered phase.

Taken together, the effects seen with annealing suggest the following. First, annealing at moderately elevated temperatures for several hours does not lead to significant interlayer interchange of molecules, as seen by the lack of change in NR for the pdpd, ppdd, and pddp samples. Second, this annealing does bring significant rearrangement of the molecules within each bilayer and the relaxation of structural asymmetry caused by the deposition. This rearrangement may be divided into two cases, that of the sample pppp which is a small sample and that of the pdpd, ppdd, and pddp samples which are larger. As noted above, the sample size has a direct effect on rod orientation. The pppp sample exhibited a complete loss of the first and second Bragg peaks in the XR data, indicating a complete loss of periodic electron density variation in the sample. This is evidence of an increased mobility for the rods in these samples, which may be due to an initial alignment which is better than that of the rods in the larger samples. Some relaxation of the larger samples also occurs, as seen by changes in, but not complete loss of, the Bragg peaks in the XR data. The exact nature of this relaxation is unclear. Lastly, there is no evidence that the PG forms a structure with hexagonal symmetry upon annealing.

Conclusions

The study of Langmuir–Blodgett–Kuhn multilayers of a novel hairy-rod polyglutamate copolymer with the complementary techniques of X-ray and neutron reflectometry reveals several aspects of their structure and change upon annealing at elevated temperature. The deposition process creates a multilayer with significant structural asymmetry with the polypeptide backbones located preferentially near the interface at the center of each bilayer. Distinctions between layers are not sharply defined, even in the as-deposited multilayers, but rather substantial interdigitation occurs between both the layers of adjacent bilayers and the layers within one bilayer.

When the multilayers are annealed, at 70 or 84 °C, the asymmetry within each bilayer induced by the deposition is relaxed irreversibly. However, there is no measurable interchange of molecules between layers and the layered structure appears to persist.

Acknowledgment. The authors thank Dr. W. Schrepp for his assistance in preparing the PG samples. Research support was provided by the Bundesministerium für Forschung und Technologie (BMFT), The University of Akron, and the National Science Foundation under Grant CTS-9110110. Computer resources were provided by the EPIC Macromolecular Modeling Center at The University of Akron. Identification of commercial products does not imply endorsement by NIST.

References and Notes

(1) Duda, G.; Wegner, G. *Makromol. Chem., Rapid Commun.* **1988**, *9*, 495.
(2) Duda, G.; Schouten, A. J.; Arndt, T.; Lieser, G.; Schmidt, G. F.; Bubeck, C.; Wegner, G. *Thin Solid Films* **1988**, *159*, 221.
(3) Hickel, W.; Duda, G.; Jurich, M.; Krohl, T.; Rochford, K.; Stegeman, G. I.; Swalen, J. D.; Wegner, G.; Knoll, W. *Langmuir* **1990**, *6*, 1403. Vogel, A.; Hoffmann, B.; Schwiegk, S.; Wegner, G. *Sens. Acuators* **1991**, *4*, 65. Mathauer, K.; Mathy, A.; Bubeck, C; Wegner, G.; Hickel, W.; Scheunemann, U. *Thin Solid Films* **1992**, *210/211*, 449.
(4) Watanabe, J.; Ono, H.; Uematsu, I.; Abe, A. *Macromolecules* **1985**, *18*, 2141. Ono, H.; Watanabe, J.; Abe, A. *Kobunshi Ronbunshu* **1988**, *45*, 69.
(5) Yamanobe, T.; Tsukahara, M.; Komoto, T.; Watanabe, J.; Ando, I.; Uimatsu, I.; Deguchi, K.; Fujito, T.; Imanari, M. *Macromolecules* **1988**, *21*, 48.
(6) Watanabe, J.; Takashina, Y. *Macromolecules* **1991**, *24*, 3423.
(7) Watanabe, J.; Fukuda, Y.; Gehani, R.; Uematsu, I. *Macromolecules* **1984**, *17*, 1004.
(8) Tsujita, Y.; Ojika, R.; Tsuzuki, K.; Takizawa, A.; Kinoshita, T. *J. Polym. Sci., Part A: Polym. Chem.* **1987**, *25*, 1041.
(9) Tsujita, Y.; Ojika, R.; Takizawa, A.; Kinoshita, T. *J. Polym. Sci., Part A: Polym. Chem.* **1990**, *28*, 1341.
(10) Nizzoli, F.; Hillebrands, B.; Lee, S.; Stegeman, G. I.; Duda, G.; Wegner, G.; Knoll, W. *Phys. Rev. B* **1989**, *40*, 3323.
(11) Chi, L.; Eng, L.; Graf, K.; Fuchs, H. *Langmuir* **1992**, *8*, 2255.
(12) Tsukruk, V. V.; Foster, M. D.; Reneker, D. H.; Schmidt, A.; Knoll, W. *Langmuir* **1993**, *9*, 3538.
(13) Tsukruk, V. V.; Foster, M. D.; Reneker, D. H.; Schmidt, A.; Wu, H.; Knoll, W. *Macromolecules* **1994**, *27*, 1274.
(14) Mathy, A.; Mathauer, K.; Wegner, G.; Bubeck, C. *Thin Solid Films* **1992**, *215*, 98.
(15) Mathauer, K. Ph.D. Thesis, University of Mainz, Mainz, Germany, 1991.
(16) Arndt, T.; Wegner, G. *Optical Techniques to Characterize Polymer Systems*; Elsevier Science: Amsterdam, 1989; p 41.
(17) Bovey, F. A. *Macromolecules: An Introduction to Polymer Science*; Academic Press: New York, 1979; p 445.
(18) Foster, M. D.; Stamm, M.; Reiter, G.; Hüttenbach, S. *Vacuum* **1990**, *41*, 1441.
(19) Kiessig, H. *Ann. Phys.* **1931**, *10*, 715.
(20) Lekner, J. *Theory of Reflection*; Martinus Nijhoff Publishers: Boston, 1987.
(21) Parrat, L. G. *Phys. Rev.* **1959**, *95*, 359.
(22) Névot, L.; Croce, P. *Rev. Phys. Appl. (Paris)* **1980**, *15*, 761.
(23) Schmidt, A.; Mathauer, K.; Reiter, G.; Foster, M.; Stamm, M.; Wegner, G.; Knoll, W. Accepted in *Langmuir*.
(24) Pauling, L.; Corey, R. B. *Proc. Natl. Acad. Sci. (U.S.A.)* **1951**, *37*, 235. Also calculations using molecular simulations performed with the commercial software package POLYGRAF from BioDesign, Inc.
(25) Bates, F. S.; Wignall, G. D.; Koehler, W. C. *Phys. Rev. Lett.* **1985**, *55*, 2425.
(26) Bates, F. S.; Wignall, G. D. *Macromolecules* **1986**, *19*, 932.
(27) Buckingham, A. D.; Hentschel, H. G. E. *J. Polym. Sci., Polym. Phys. Ed.* **1980**, *18*, 853.
(28) Bates, F. S.; Wignall, G. D. *Phys. Rev. Lett.* **1986**, *57*, 1429.
(29) Singh, R. R.; Van Hook, W. A. *Macromolecules* **1987**, *20*, 1855.
(30) English, A. D.; Smith, P.; Axelson, D. E. *Polymer* **1985**, *26*, 1523.
(31) Dorset, D. *Macromolecules* **1991**, *24*, 6521.
(32) Doi, M.; Edwards, S. F. *The Theory of Polymer Dynamics*; Oxford Press: New York, 1989.
(33) Embs, F. W.; Wegner, G.; Neher, D.; Albouy, P.; Miller, R. D.; Willson, C. G.; Schrepp, W. *Macromolecules* **1991**, *24*, 5068.
(34) Embs, F. W. Ph.D. Thesis, University of Mainz, Mainz, Germany, 1990.